Accepted Manuscript

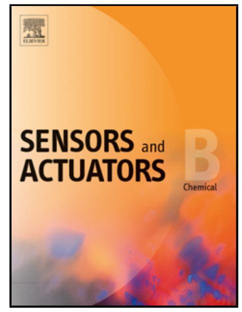

Title: NH_3 sensing property and mechanisms of quartz surface acoustic wave sensors deposited with SiO_2, TiO_2, and SiO_2-TiO_2 composite films

Authors: Yongliang Tang, Dongyi Ao, Wei Li, Xiaotao Zu, Sean Li, Yong Qing Fu

PII: S0925-4005(17)31409-0
DOI: http://dx.doi.org/doi:10.1016/j.snb.2017.07.195
Reference: SNB 22854

To appear in: *Sensors and Actuators B*

Received date: 11-3-2017
Revised date: 26-7-2017
Accepted date: 27-7-2017

NH_3 sensing property and mechanisms of quartz surface acoustic wave sensors deposited with SiO_2, TiO_2, and SiO_2-TiO_2 composite films

Yongliang Tang[1], Dongyi Ao[2], Wei Li[2], Xiaotao Zu[1,2,], Sean Li[4,*], Yong Qing Fu[3,*]*

[1]Institute of Fundamental and Frontier Sciences, University of Electronic Science and Technology of China, Chengdu 610054, P.R. China

[2]School of Physical Electronics, University of Electronic Science and Technology of China, Chengdu, 610054, People's Republic of China

[3]Mathematics Physics and Electrical Engineering, Northumbria University, Newcastle upon Tyne, NE1 8ST, UK

[4]School of Materials Science & Engineering, UNSW SYDNEY, NSW 2052, AUSTRALIA

[*]Correspondence to: Xiaotao Zu: xtzu@uestc.edu.cn; Sean Li: sean.li@unsw.edu.au; Yongqing Fu: richard.fu@northumbria.ac.uk

Highlights

- Hydroxyls groups play critical roles in NH_3 sensing
- Negative frequency shift is contributed from mass loading on films

- Positive frequency shift is contributed from condensation of hydroxyls groups
- SiO_2-TiO_2 based SAW sensors have a high response of 2 KHz when exposed to 1 ppm NH_3

Abstract:

Pristine SiO_2, TiO_2 and composite SiO_2-TiO_2 films of 200 nm thick were coated on surface of quartz acoustic wave (SAW) sensors with sol-gel and spin coating technique. Their performance and mechanisms for sensing NH_3 were systematically investigated. Sensors made with the TiO_2 and SiO_2-TiO_2 films showed positive frequency shifts, whereas SiO_2 film exhibits a negative frequency shift to NH_3 gas. it is believed that the negative frequency shift was mainly caused by the increase of NH_3 mass loading on the sensitive film while the positive frequency shift was associated to the condensation of the hydroxyl groups (-OH) on the film making the film stiffer and lighter, when exposed to NH_3 gas. It demonstrated that humidity played a significant factor on the sensing performance. Comparative studies exhibited that the sensor based on the composite SiO_2-TiO_2 film had a much better sensitivity to NH_3 at a low concentration level (1 ppm) with a response of 2 KHz, and also showed fast response and recovery, excellent selectivity, stability and reproducibility.

Key words: SAW sensor; hydroxyl groups; mass loading; elastic modulus

1. Introduction

Ammonia is an important industrial forming gas used in various fields including pharmaceuticals and chemical industries as well as national security [1-8]. However, it is flammable and poisonous that can cause seizures, collapse, lung damage, blindness, coma, and even death [9-12]. Therefore, determining the leakage of ammonia in ambient environment becomes critical. To achieve this goal, various types of ammonia sensors, such as metal oxide semiconductor sensors, electrochemical sensors and surface acoustic wave (SAW) sensors were developed, [13-17]. Benefiting from the significant development of RF and crystal technologies, surface acoustic wave techniques (SAWTs) are playing important roles in our daily life [18-21]. Among the various SAWTs, such as microfluidic and RFID techniques, the SAW sensor technique has been attracting more attention due to the serious air pollution in recent years [22-25]. SAW sensors have advantages of high sensitivity, high speed, good reliability, high accuracy, and low cost, which are suitable for practical applications. A SAW sensor is essentially an RF oscillator. The core part of such a sensor is a SAW resonator coated with a sensitive film layer to act as frequency-changing component through the adsorption/chemical binding of ammonia molecules. The central frequency of the resonator can alter the conductivity (electric loading), effective mass (mass loading) or elastic modulus/density/viscosity (elastic loading) of the film [26-29]. Hence, for a good SAW based NH_3 sensor, the sensitive film should be sensitive to one or all these variations when exposed to NH_3 gas. For example, Raj et al. reported a quartz SAW sensor with a ZnO film layer, which showed a negative frequency shift attributed to the variations of mass and elastic modulus of the ZnO film when exposed to NH_3 [30]. Chen et al. showed a quartz SAW NH_3 sensor with a Pt doped polypyrrole sensitive film, and they attributed the positive frequency shift to the variation of conductivity of film [31]. Similar work about either positive or negative frequency shift of the SAW NH_3 sensor has been reported in many references [32-34].

The pristine SiO_2 and TiO_2 as well as the composite SiO_2-TiO_2 films have been extensively studied because of their extraordinary optical, catalytic, electrical and mechanical properties [35-

38]. However, their gas sensing performance for NH_3 has not been widely exploited. Although various methodologies including magnetron sputtering, chemical vapor deposition and thermal oxidation techniques have been used to fabricate the films [39-41], sol-gel methodology is the most cost-effective technique.

It is believed that a large amount of hydroxyl groups (-OH) existed on the SiO_2 and TiO_2 and composite SiO_2-TiO_2 films prepared with sol-gel technology [42,43], even after their calcination [44,45]. Since these hydroxyl groups are hydrophilic, H_2O in the ambient environment can be easily absorbed on the surface of the films to act as the positive sites for absorbing NH_3. The extremely high solubility of NH_3 in H_2O results in the films to be much heavier. In addition, it has been reported that the hydroxyl groups can also be catalyzed into condensation by NH_3 [46-48]. Consequently, when these films (both pristine and calcined) are exposed to NH_3, they may also become stiffer and lighter because of the condensation of the hydroxyl groups, therefore, they could be explored as good sensing films for SAW NH_3 sensors.

In this work, we deposited the SiO_2, TiO_2 and SiO_2-TiO_2 films on the surfaces of the as-fabricated quartz surface acoustic wave (SAW) sensors. The sensing mechanisms for ammonia (NH_3) were systematically studied. The as-deposited films were rich of the hydroxyl groups, which is an advantageous characteristic for the NH_3 sensing. The experimental results demonstrate that the sensor coated by SiO_2-TiO_2 film is much more sensitive than those made with a layer of its individual components. Also the humidity was found to have significant influence on the sensing behavior and the reasons have been identified.

2. Material and methods

2.1 Materials

Tetraethoxysilanc (TEOS), Tetrabutyl titanate (TBT), ethanol, and ammonia (analytic pure liquid, 25 wt%) were all analytically pure and purchased from Chengdu Kelong Chemical Reagent Factory, China. Standard NH_3 (2 vol%), H_2S (2 vol%), H_2 (2 vol%), CO (2 vol%), CH_4 , (2 vol%) and C_2H_5OH (2 vol‰) gases in dry air were purchased from the National Institute of Measurement and Testing Technology, China. SAW resonator fabricated on ST-cut quartz consists of the input and output interdigital transducers (IDTs, 30 pairs each) and 100 pairs of reflection gratings. The IDTs and reflection gratings with a periodicity of 16 μm were fabricated by conventional lithography technique on 200 nm thick Al thin film that was deposited by magnetron sputtering. The aperture of the IDTs was 3 mm and the central frequency of the resonator was designed as 200 MHz.

2.2 Preparation of sols

SiO_2, TiO_2 and SiO_2-TiO_2 sols were prepared by sol-gel technique. SiO_2 sol was prepared by a modified Stober method [49]. In a typical procedure, the ethanol (analytic pure), TEOS (high pure), deionized water, and ammonia (analytic pure liquid, 25 wt%) were successively added into a Bunsen flask with a molar ratio of 1: 3.25:37: 0.17 under a continual magnetic stirring. The obtained solution was stirred at 30 °C for 2 hrs and aged for 7 days to obtain the colloidal silica sol with a concentration of 0.5 mol/L. TiO_2 sol was prepared using the following procedures. TBT of 2 g was firstly added into a beaker containing 20 ml ethanol under the magnetic stirring for 30 minutes, and then 0.25 ml ammonia (25-28 wt%) was added into the beaker dropwise under a vigorous stirring. The obtained solution was then aged for 1 day to get the colloidal TiO_2 sol. The mixture of SiO_2-TiO_2 sol was prepared with the volume ratio of 1: 1 under the magnetic stirring for 30 minutes.

2.3 Preparation of films

The SiO_2, TiO_2 and mixed SiO_2-TiO_2 sols were coated onto the SAW resonators (and K9 glasses, which used for electrical and film thickness characterization) using a multi-spin-coating process (3-cycles), with a speed of 3000 r/min for 30 s in each cycle. The coated quartz substrates were immediately annealed at 300 °C for about 10 min and then at 450 °C for 2 hrs in ambient atmosphere. Finally, the coated resonators were connected to the equivalent circuit to build SAW sensors (together with the oscillating circuits), as shown in Fig. 1.

2.4 Characterizations

Rigaku D/max-2400 X-ray diffractometer was used to characterize the crystallinity of the prepared films. The morphology of the as-prepared films was characterized by field-emission scanning electron microscopy (SEM, FEI Inspect F). An FTIR Spectrometer (Nicolet 6700) was used to collect the infrared absorption spectra of the prepared films. A source meter (Keithley 2400) was used to measure the sheet conductivity of the films coated on K9 glass. An ellipsometer (TP77) was used to determine the thickness of prepared films on K9 glass.

To conduct the gas sensing measurement, the ambient temperature was kept at 25 °C and the relative humidity (RH) was controlled by a humidifier and a mass flow controller which controls the flow rate of dry air. During the measurement, the environment RH was adjusted to the desired values. The sensors were connected to a frequency counter (Agilent 53132A) to monitor the dynamic oscillating frequency of sensor. The sensor was mounted in a chamber with a volume of 2 L. A syringe was used to inject the standard ammonia gases into the testing chamber and the response of the sensor was recorded (Fig. 2). The concentration (with fixed values of 1, 2, 5, 10, 20 and 40 ppm for each test) of the NH_3 gases was controlled by adjusting the injecting volumes from the syringe (0.1, 0.2, 0.5, 1, 2, and 4 ml). When the response of sensor was stable, the chamber was opened, and thus the sensor was exposed to the ambient atmosphere to test its recovery performance. The response of sensor was defined as $\Delta f = f_s - f_0$, where f_s and f_0 are the oscillating frequencies in testing gas and atmosphere, respectively. Thus, Δf is positive if the oscillating frequency increases when the sensor was exposed to testing gas and vice versa. The time taken for the sensor to achieve 90% of the total frequency shift was defined as the response time in the case of gas adsorption or the recovery time in the case of gas desorption.

3. Results and discussion

3.1 Characterization of prepared films

SEM surface morphology images of SiO_2, TiO_2 and SiO_2-TiO_2 films are shown in Fig. 3. The SiO_2 film was composed of SiO_2 nanoparticles with an average diameter of ~40 nm. Lots of pores can be found on the film. The TiO_2 film show a dense structure without apparent pores observed, and the particles size of TiO_2 is small (~15 nm). The SiO_2-TiO_2 film has a porous structure, and the pores and cracks are large and the particles size is larger than that of SiO_2 film, with an average diameter of ~60 nm. The pores and cracks may act as the paths for gas molecules to diffuse into the films, hence, more porous surfaces can act as the absorption sites for gas molecules, which is beneficial for sensing.

XRD patterns of the SiO_2, TiO_2 and SiO_2-TiO_2 films are shown in Fig. 4. XRD pattern of the SiO_2 film shows a broad peak at about 23°, which is the typical character of amorphous SiO_2. Rutile TiO_2 was also evidenced in the XRD spectra. XRD pattern of SiO_2-TiO_2 film is similar to that of TiO_2 film, however, the intensity of all peaks is weaker. Besides, there is also a broad peak at about 23°. Hence, it clearly demonstrates that amorphous SiO_2 and Rutile TiO_2 co-existed in the as-prepared SiO_2-TiO_2 film.

The typical FTIR spectra of SiO_2, TiO_2 and SiO_2-TiO_2 films are presented in Fig. 5. In the high wave number spectral range, broad bands between 3600 and 2800 cm^{-1} can be observed in all the three spectra, which can be assigned to fundamental stretching vibration modes of different OH hydroxyl groups (free or bounded) [42]. The band at 1630 cm^{-1} is associated to molecular water, and the band at ~960 cm^{-1} is attributed to stretching mode of non-bridging oxygen atoms, e.g., Si-OH and Ti-OH. In the spectra of SiO_2 (Fig. 5a), various bands at 427, 790, and 1070 cm^{-1} are associated with SiO_2, corresponding to its transverse optical (TO) modes. The shoulder at 1210 cm^{-1} is associated with the longitudinal optical LO3 mode of SiO_2 while the shoulder at 3650 cm^{-1} is derived from SiO-H stretching [45]. In the spectra of TiO_2 (Fig. 5b), there is a broad and intense band in the range of 400-800 cm^{-1}, which can be assigned to Ti-O and Ti-O-Ti groups. The band at 3737 cm^{-1} can be ascribed to surface Ti-OH groups, and the band ranging from 1300 to 1500 cm^{-1} can be assigned to the residual carbon [50]. From Fig. 5c, the appearance of both SiO_2 and TiO_2 spectra demonstrates the co-existence of SiO_2 and TiO_2 in the tested sample.

From FTIR results, it clearly shows that there are hydroxyl groups on all the three films, and the hydroxyl groups can absorb H_2O in ambient environment. These absorbed water molecules can attract NH_3, making the film heavier when exposed to NH_3. The absorbed NH_3 can also facilitate the condensation of hydroxyl groups, making the films stiffer and lighter. Hence these films could be explored as the good sensing films for SAW NH_3 sensors.

Table 1 listed the average film thickness and sheet conductivity of films. All the films have an average thickness of ~200 nm and the sheet conductivity is lower than 10^{-9} S/square.

.Gas sensing properties and sensing mechanisms

Fig. 6a shows the responses of the sensors based on SiO_2, TiO_2 and SiO_2-TiO_2 films (designated as Sensor 1, Sensor 2 and Sensor 3, respectively) when exposed to 10 ppm NH_3. Sensor 2 and Sensor 3 exhibit positive frequency shifts (Δf), whereas Sensor 1 exhibits a negative frequency shift. Moreover, Sensor 3 shows the strongest response. The frequency shifts of the SAW sensors are contributed by three factors: the sheet conductivity (electric loading), the mass loading on the film (mass loading) and Young's modulus (elastic loading).

The relationship between the frequency shift (Δf) and the electric loading is given below [27],

$$\Delta f = -f_0 \times \frac{K^2}{2} \times \Delta\left(\frac{1}{1+\left(\frac{V_0 C_s}{\sigma_s}\right)^2}\right) \qquad (1)$$

Where, f_0 = 200 MHz, V_0 = 3158 m/s (for substrate of ST-cut quartz), K^2 = 0.0011, C_s = 0.5 pF/cm are the unperturbed oscillation frequency of the sensor, the unperturbed SAW velocity on the SAW resonator, electromechanical coupling coefficient, the capacitance per unit length of the SAW resonator fabricated on a ST-cut quartz substrate, respectively. σ_s is the sheet conductivity of the sensing film, which is lower than 10^{-9} S square for all the films used in our experiment (Table 1). In our experiment, σ_s values of all the sensing films increase by exposure to NH_3, and the rate of increase is less than 4 times as shown in Fig. 6b (the response was defined as R = R_{air}-R_{gas}/R_{gas}, where R_{air} is the film resistance in ambient air, R_{gas} is the film resistance in a mixture of NH_3 and air). The calculated values of V_0C_s/σ_s in Equation (1) are listed in Table 1, either with or without NH_3 in the environment. According to Equation (1), the calculated values of Δf (Δf_e) contributed from the electric loading are 2.2×10^{-5}, 3.4×10^{-2} and 2.5×10^{-3} Hz for Sensor 1, Sensor 2 and Sensor 3 respectively when exposure to NH_3 of 10 ppm. These are far smaller than the experimental value of Δf. Thus, it can be concluded that the contribution of electric loading is not significant. The Δf is mainly caused by the mass and elastic loadings.

The mass loading on the film changes the frequency of sensors follows Equation (2) [30],

$$\Delta f = (k_1 + k_2) \times f_0^2 \times \Delta\rho_s \qquad (2)$$

where $k_1 = -8.7\times10^{-8}$ m^{2}skg^{-1} and $k_2 = -3.9\times10^{-8}$ m^{2}skg^{-1} which are substrate material constants of S–T cut quartz. $\Delta\rho_s$ is the change of areal density of the sensing film on the SAW device when exposed to NH_3. Note that k_1 and k_2 are both negative in signs, therefore a positive change $\Delta\rho_s$ will lead to a negative value of Δf.

The relationship between the frequency shift and the elastic loading is given by [30],

$$\Delta f = p\Delta E \qquad (3)$$

Where *p* is a positive constant, *ΔE* is the change of the elastic modulus of sensing film when exposed to NH_3. Note that when *ΔE* is positive (i.e., the stiffness of film increases), the sensor would show a positive shift.

The FTIR results verified that the hydrophilic hydroxyls formed on SiO_2, TiO_2 and SiO_2-TiO_2 films. Hence, the H_2O molecules in the ambient environment are easily absorbed on the films (Fig. 7a). Fig. 7 schematically illustrates two potential variations occurred on the film surface by interacting with NH_3. (1) The absorbed H_2O can act as the positive sites for absorbing NH_3 due to the high solubility of NH_3 in H_2O, making the films much heavier (Fig. 7b). Hence, the frequency of sensor has a negative shift [Equation (2)]. (2) The hydroxyls on the films are catalyzed by absorbed NH_3 to become condensation (Fig. 7c). As a result, the films will become stiffer and lighter. Consequently, the *Δf* contributed by the Variation (2) should be positive according to Equations (2) and (3).

For Sensor 1, Variation (1) is responsible for the negative *Δf shift* whereas the Variation (2) is the main mechanism for Sensor 2 and Sensor 3 due to their positive *Δf*. To further understand why the response of Sensor 3 is much stronger than Sensor 2 and also the influence of humidity on the as-prepared sensors, the relative humidity (RH) was varied from 5% to 70% to reveal the underlying principle in our experiments. The results of these experiments are summarized in Table 2. All the sensors showed a negative frequency shift when RH was increased. This is because more water has been absorbed on the films due to the hydrophilic hydroxyls on the surface of films, hence the mass loading on the films increases when the RH is increased. In addition, Sensor 1 and Sensor 3 are much more sensitive to RH. Consequently, it can be concluded that much more water will be absorbed on SiO_2 and SiO_2-TiO_2 films. The absorbed water acts as the positive site for absorbing NH_3 onto the films, thus increasing the concentration of NH_3 on the film. As a result, the concentration of NH_3 is much higher on SiO_2-TiO_2 film than that on TiO_2 film, making Sensor 3 much more sensitive than Sensor 2. To confirm this conclusion, responses of sensors to NH_3 under different RHs were also measured and the results are shown in Fig. 8a-c. Clearly the responses of all sensors increase with the RH value, thus supporting the aforementioned results.

Both Variations (1) and (2) may be responsible to the sensing performance. To compare the differences of the influence of Variations (1) and (2) on the responses of the sensors, we analyzed the recovery curves of Sensor 1 and Sensor 2, as shown in Fig. 8d. Opposite to the response process, the recovery processes of Variations (1) and (2) caused positive and negative frequency shifts, respectively. For Sensor 2, the frequency kept decreasing for ~30 s during whole recovery process, indicating that the recovery [in Variation (2)] occurred for at least 30 s. Since if it is less than 30 s, the frequency would be either stabilized or increased because of the recovery in Variation (1). Based on above result, it is clear that the recovery duration of a sensor lasted for at least 30 s if the Variation (2) contributes to the response of the sensor. However, the recovery of Sensor 1 lasted for only ~15 s (Fig. 8d). Hence, we can conclude that the Variation

(1) has dominant influence to the response to NH_3 for Sensor 1 and Variation (2) has little contribution, whereas the Variation (2) contributes much more to the performance of Sensor 2 and Sensor 3. During the sensing tests of Sensor 2 and Sensor 3, since the water contents on the TiO_2 and SiO_2-TiO_2 films are about 9.27 and 1.62 times less than that on the SiO_2 film (Table 2), respectively, the Variation (1) caused by NH_3 on these films is not higher than that on SiO_2 film. Therefore, the response from Variation (1) is not larger than -400 Hz (Fig. 8a, the response of Sensor1 at RH=40%), which is 5 and 20 times lower than the practical responses of Sensor 2 and Sensor 3. Therefore, we concluded that the responses of Sensor 2 and Sensor 3 to NH_3 should be mainly due to the Variation (2).

Since the Sensor 3 has the best performance in the NH_3 sensing, the following tests were all done using the Sensor 3 in an RH of 40 % at 25 °C. Fig. 9a shows the dynamic response of the Sensor 3, and the sensor was able to detect NH_3 gas concentration as low as 1 ppm with a response of 2 KHz. In addition, the frequency response increased when the gas concentration was increased from 1 ppm to 40 ppm. Fig. 9c shows the response and recovery times as a function of NH_3 gas concentration. The response time changed insignificantly whereas the recovery time was increased from 60 s to 140 s when the NH_3 gas concentration was increased from 1 ppm to 40 ppm.

As discussed, the response of Sensor 3 is mainly derived from the Variation (1) contributed by the condensation of hydroxyls on SiO_2-TiO_2 film, which is facilitated by the adsorption of NH_3. Hence, we believe that the Sensor 3 has a good selectivity to NH_3, since the other mostly common gases may show no catalytic action for the condensation of hydroxyls. To confirm this, the Sensor 3 was also exposed to 10 ppm H_2, CO, CH_4, H_2S and C_2H_5OH gases using the same methodology as described before, and the results are shown in Fig. 9d. The Sensor 3 showed no significant responses to 10 ppm H_2, CO, CH_4, H_2S, and shows only ~200 Hz frequency shift to 10 ppm C_2H_5OH, which is 50 times weaker than its response to NH_3, indicating the good selectivity of Sensor 3.

The reproducibility and long term stability of Sensor 3 were also investigated. Sensor 3 was exposed to NH_3 of 10 ppm for response and recovery for 4 cycles (Fig. 9e), the fluctuation of frequency shift is less than 5% for the 4 consecutive cycles, indicating good reproducibility. 5 individual tests were conducted in 50 days for investigation of the long term stability of Sensor 3. In each test, the Sensor 3 was consecutively exposed to NH_3 of 1, 10 and 40 ppm for response and recovery, the total time for a single test was about 15 minutes. The test was conducted every 10 days. The result of the five tests is shown in Fig. 9f. Clearly the sensor shows stable responses to NH_3 gas of various concentrations for 50 days.

4. Conclusion

In summary, the quartz SAW sensors with SiO_2, TiO_2 and SiO_2-TiO_2 films were fabricated and used for the applications of sensing NH_3. All the sensors showed good responses to NH_3. The sensors based on TiO_2 and SiO_2-TiO_2 films showed positive responses which are mainly due to the condensation of hydroxyls catalyzed by NH_3, making the film stiffer and lighter. in contrast, the sensor based on SiO_2 film showed a negative response, which is mainly due to the increase of the mass loading caused by absorbed NH_3. In addition, the humidity was found to be significantly influential to the response of sensors because the water absorbed on the film surface acted as the active site to absorb NH_3, making the sensors more sensitive to NH_3. The sensor based on SiO_2-TiO_2 film showed the best performance to NH_3, and could detect 1 ppm NH_3 with a response of 2 KHz. Moreover, this sensor also showed excellent selectivity, stability, and reproducibility at room temperature.

Acknowledgements:

This study was supported financially by the NSAF Joint Foundation of China (U1630126, U1230124). Richard Y.Q. Fu would like to thank the UK Engineering and Physical Sciences Research Council (EPSRC) for support under grant EP/L026899/1 and Knowledge Transfer Partnership No KTP010548.

References

[1] S.B. Riffat, C.F. Afonso, A.C. Oliveira, D.A. Reay, Natural refrigerants for refrigeration and air-conditioning systems, Appl. Therm. Eng. 17(1997) 33-42.

[2] C.F. Ibbotson, R. Mansbridge, A.H. Adamson, Commercial experience of treating straw with ammonia, Anim. Feed Sci. Tech. 10 (1984) 223-228.

[3] E. Stokstad, Ammonia pollution from farming may exact hefty health costs, Science 2014 343 (2014) 238-238.

[4] R.A. Michaels, Emergency planning and the acute toxic potency of inhaled ammonia. Eenviron, Health Persp. 107 (1999) 617.

[5] C.F. Eno, G.B. William, M.G. Joseph, The effect of anhydrous ammonia on nematodes, fungi, bacteria, and nitrification in some Florida soils, Soil Sci. Soc. Am. J. 19 (1955) 55-58.

[6] J.M. Bremner, G.A. Breitenbeck, A.M. Blackmer, Effect of anhydrous ammonia fertilization on emission of nitrous oxide from soils, J. Environ. Qual. 10 (1981) 77-80.

[7] W. Ament, J.R. Huizenga, E. Kort, T.W. Van Der Mark, R.G. Grevink, G.J. Verkerke, Respiratory ammonia output and blood ammonia concentration during incremental exercise, Int. J. Sports Med. 20 (1999) 71-77.

[8] L.R. Narasimhan, W. Goodman, C.K.N. Patel, Correlation of breath ammonia with blood urea nitrogen and creatinine during hemodialysis, P. Natl. Aca. Sci. 98 (2001) 4617-4621.

[9] L.G. Close, F.I. Catlin, A.M. Cohn, Acute and chronic effects of ammonia burns of the respiratory tract, Arch. Otolaryngol. 106 (1980) 151-158.

[10] C.M. Leung, C.L. Foo, Mass ammonia inhalational burns--experience in the management of 12 patient, Ann. Aca. Med. Singapore 21(1992)624-629.

[11] R.E. de la Hoz, D.P. Schlueter, W.N. Rom, Chronic lung disease secondary to ammonia inhalation injury: a report on three cases, Am. J. Ind. Med. 29 (1999) 209-214.

[12] R.A. Michaels, Emergency planning and the acute toxic potency of inhaled ammonia, Environ. Health Persp. 107 (1999) 617.

[13] S.Y. Wang, J.Y. Ma, Z.J. Li, H.Q. Su, N.R. Alkurd, W.L. Zhou, L. Wang, B. Du, Y. Tang, D. Ao, S. Zhang, Q. Yu, X. Zu, Surface acoustic wave ammonia sensor based on ZnO/SiO_2 composite film, J. Hazard. Mater. 285 (2015) 368-374.

[14] B. Timmer, W. Olthuis, A. Van Den Berg, Ammonia sensors and their applications—a review, Sensor. Actuat. B-Chem. 107 (2005) 666-677.

[15] D. Sil, J. Hines, U. Udeoyo, E. Borguet, Palladium nanoparticle-based surface acoustic wave hydrogen sensor, ACS Appl. Mater. Interfaces 10 (2015) 5709-5714.

[16] Y.L. Tang, Z.J. Li, J.Y. Ma, H.Q. Su, Y.J. Guo, L. Wang, B. Du, J. Chen, W. Zhou, Q.Yu, X.T. Zu, Highly sensitive room-temperature surface acoustic wave (SAW) ammonia sensors based on Co_3O_4/SiO_2 composite films, J. Hazard. Mater. 280 (2014) 127-133.

[17] N. Fourati, M. Seydou, C. Zerrouki, A. Singh, S. Samanta, F. Maurel, D.K. Aswal, M. Chehimi, Ultrasensitive and selective detection of dopamine using cobalt-phthalocyanine nanopillar-based surface acoustic wave sensor, ACS Appl. Mater. Interfaces 24 (2014) 22378-22386.

[18] X. Ding, P. Li, S.C.S. Lin, Z.S. Stratton, N. Nama, F. Guo, D. Slotcavage, X. Mao, J. Shi, F. Costanzo, T.J. Huang, Surface acoustic wave microfluidics, Lab Chip 13 (2013) 3626-3649.

[19] H. Jin, J. Zhou, X. He, W. Wang, H. Guo, S. Dong, D.Wang, Y. Xu, J. Geng, J.K. Luo, W.I. Milne, Flexible surface acoustic wave resonators built on disposable plastic film for electronics and lab-on-a-chip applications, Sci. Rep. 3 (2013) 2140.

[20] Y. Q. Fu, J. K. Luo, N. T. Nguyen, A. J. Walton, A. J. Flewitt, X. T. Zu, Y. Li, G. McHale, A. Matthews, E. Iborra, H. Du, W. I. Milne, Advances in piezoelectric thin films for acoustic biosensors, acoustofluidics and lab-on-chip applications, Prog. Mater. Sci. 89 (2017) 31-91.

[21] V. Skowronek, R.W. Rambach, T. Franke, Surface acoustic wave controlled integrated band-pass filter, Microfluid. Nanofluid. 19 (2015) 335-341.

[22] S. Johnson, T. Shanmuganantham, Design and Analysis of SAW Based MEMS Gas Sensor for the Detection of Volatile Organic Gases, Carbon 119 (2014) 0-041316.

[23] W. Jakubik, Elemental theory of a SAW gas sensor based on electrical conductivity changes in bi-layer nanostructures, Sensor. Actuat. B-Chem. 203 (2014) 511-516.

[24] Y.L. Tang, Z.J. Li, J.Y. Ma, Y.J. Guo, Y.Q. Fu, X.T. Zu, Ammonia gas sensors based on ZnO/SiO_2 bi-layer nanofilms on ST-cut quartz surface acoustic wave devices, Sensor. Actuat. B-Chem. 201 (2014) 114-121.

[25] Y.Q. Fu, J.K. Luo, X.Y. Du, A.J. Flewitt, Y. Li, G.H. Markx, A.J. Walton, W.I. Milne, Recent developments on ZnO films for acoustic wave based bio-sensing and microfluidic applications: a review, Sensor. Actuat. B-Chem. 143(2010) 606-619.

[26] R. Lucklum, C. Behling, P. Hauptmann, Role of mass accumulation and viscoelastic film properties for the response of acoustic-wave-based chemical sensors, Anal. Chem. 71 (1999) 2488-2496.

[27] A.J. Ricco, S.T. Martin, T.E. Zipperian, Surface acoustic wave gas sensor based on film conductivity changes, Sensor. Actuat. 8 (1985) 319-333.

[28] D.Y. Gallimore, P.J. Millard, M. Pereira da Cunha, Monitoring Polymer Properties Using Shear Horizontal Surface Acoustic Waves, ACS Appl. Mater. Interfaces 10 (2009) 2382-2389.

[29] Y. Tang, Z. Li, J. Ma, L. Wang, J. Yang, B. Du, Q. Yu, X. Zu, Highly sensitive surface acoustic wave (SAW) humidity sensors based on sol–gel SiO_2 films: Investigations on the sensing property and mechanism, Sensor. Actuat. B-Chem. 215 (2015) 283-291.

[30] V.B. Raj, H. Singh, A.T. Nimal, M.U. Sharma, M. Tomar, V. Gupta, Distinct detection of liquor ammonia by ZnO/SAW sensor: Study of complete sensing mechanism, Sensor. Actuat. B-Chem. 238 (2017) 83-90.

[31] X. Chen, D.M. Li, S.F. Liang, S. Zhan, M. Liu, Gas sensing properties of surface acoustic wave NH_3 gas sensor based on Pt doped polypyrrole sensitive film, Sensor. Actuat. B-Chem. 177 (2003) 364-369.

[32] J.W. Grate, Acoustic wave microsensor arrays for vapor sensing, Chem. Rev. 100 (2000) 2627-2648.

[33] W. Buff, M. Rusko, E. Goroll, J. Ehrenpfordt, T. Vandahl, Universal pressure and temperature SAW sensor for wireless applications, IEEE Ultrasonics Symposium Proceedings 1 (1997) 359-362.

[34] M. Rapp, J. Reibel, S. Stier, A.Voigt, J. Bahlo, SAGAS: gas analyzing sensor systems based on surface acoustic wave devices-an issue of commercialization of SAW sensor technology, IEEE Frequency Control Symposium (1997) 129-132.

[35] D.G. Cahill, T.H. Allen, Thermal conductivity of sputtered and evaporated SiO_2 and TiO_2 optical coatings, Appl. Phys. Lett. 65 (1994) 309-311.

[36] S.H Jeong, J.K. Kim, B.S. Kim, S.H. Shim, B.T. Lee, Characterization of SiO_2 and TiO_2 films prepared using rf magnetron sputtering and their application to anti-reflection coating, Vacuum 76 (2004) 507-515.

[37] I. Sopyan, S. Murasawa, K. Hashimoto, A. Fujishima, Highly efficient TiO_2 film photocatalyst. Degradation of gaseous acetaldehyde, Chem. Lett. 23 (1994) 723-726.

[38] M. Langlet, M. Burgos, C. Coutier, C. Jimenez, C. Morant, M. Manso, Low temperature preparation of high refractive index and mechanically resistant sol-gel TiO_2 films for multilayer antireflective coating applications, J. Sol-Gel Sci. Technol. 22 (2011) 139-150.

[39] J. Szczyrbowski, G. Bräuer, G. Teschner, A. Zmelty, Antireflective coatings on large scale substrates produced by reactive twin-magnetron sputtering, J. Non-cryst. Solids 218 (1997) 25-29.

[40] D. Luca, L.S. Hsu, Structural evolution and optical properties of TiO_2 thin films prepared by thermal oxidation of PLD Ti films, J. Optoelectron. Adv. Mater. 5 (2003) 835-840.

[41] T. Kogure, T. Umezawa, Y. Kotani, A. Matsuda, M. Tatsumisago, T. Minami, Formation of TiO_2 (B) Nanocrystallites in Sol- Gel- Derived SiO_2- TiO_2 Film, J. Am. Ceram. Soc. 82 (1999) 3248-3250.

[42] M. Burgos, M. Langlet, Condensation and densification mechanism of sol-gel TiO_2 layers at low temperature, J. Sol-gel Sci. Technol. 16 (1999) 267-276.

[43] T.M. Parrill, Transmission infrared study of acid-catalyzed sol-gel silica coatings during room ambient drying, J. Mater. Res. 7 (1992) 2230-2239.

[44] J. Yu, X. Zhao, Q. Zhao, Effect of surface structure on photocatalytic activity of TiO_2 thin films prepared by sol-gel method, Thin solid films 379 (2000) 7-14.

[45] N. Primeau, C. Vautey, M. Langlet, The effect of thermal annealing on aerosol-gel deposited SiO_2 films: a FTIR deconvolution study, Thin Solid Films 310 (1997) 47-56.

[46] F.P. Belleville, H.G. Floch, Ammonia hardening of porous silica antireflective coatings, International Symposium on Optics, Imaging, and Instrumentation (1994) 25–32.

[47] G. Wu, J. Wang, J. Shen, T. Yang, Q. Zhang, B. Zhou, Z. Deng, F. Bin, D. Zhou, F. Zhang, Properties of sol–gel derived scratch-resistant nano-porous silica films by a mixed atmosphere treatment, J. Non-cryst. Solids 275 (2000) 169-174.

[48] X. Li, S.A. Jun, scratch-resistant and hydrophobic broadband antireflective coating by sol–gel method, Thin Solid Films 519 (2011) 6236-6240.

[49] W. Stöber, A. Fink, E.J. Bohn, Controlled growth of monodisperse silica spheres in the micron size range, Colloid Interface Sci. 26 (1968) 62–69.

[50] K. Kandori, M. Oketani, Y. Sakita, M. Wakamura, FTIR studies on photocatalytic activity of Ti (IV)-doped calcium hydroxyapatite particles, J. Mol. Catal. A-Chem. 360 (2012) 54-60.

Yongliang Tang obtained his B.S. degree in School of Physical Electronics, University of Electronic Science and Technology of China in 2011. He is a Ph.D. student in Institute of Fundamental and Frontier Sciences at University of Electronic Science and Technology of China. His present interests include applications of nanomaterials and functional thin films for sensors and surface acoustic wave (SAW) devices.

Dongyi Ao btained his B.S. degree in School of Management and Economics, University of Electronic Science and Technology of China in 2012. He is a Ph.D. student in School of Physical Electronics at University of Electronic Science and Technology of China. His present interests include applications of nanomaterials and functional thin films for sensors and surface acoustic wave (SAW) devices, graphene preparation and applications.

Wei Li obtained his B.S. degree in School of Physical and Electronics, Henan University in 2012. He is a Master Degree Candidate in School of Physical Electronics at University of Electronic Science and Technology of China. His current research interests focus on sensing devices using acoustic wave technology, microfluidics and interaction between laser and solid material.

Xiaotao Zu received his Ph.D. degree from Sichuan University in 2002. He is a Professor in School of Physical Electronics at University of Electronic Science and Technology of China. His research interests include photo electric materials, smart materials, composite nanomaterials and their industrial applications.

Sean Li is a Professor in School of Materials Science & Engineering, UNSW SYDNEY. His research interests include advanced electronic, photonic and multifunctional materials.

Richard Yong-Qing Fu received his Ph.D. degree from Nanyang Technological University, Singapore in 1999, and now worked in Mathematics Physics and Electrical Engineering, Northumbria University, UK. His recent research has been focusing on microactuators, microsensors and microfluidic devices based on smart functional thin films.

Figure captions

Figure 1. The schematic diagram (a) and a photo (b) of a SAW sensor.

Figure 2. The setup of the experimental system.

Figure 3. The SEM surface morphology images of SiO_2 (a), TiO_2 (b) and SiO_2-TiO_2 (c) films.

Figure 4. The XRD patterns of pristine SiO_2, TiO_2 and SiO_2-TiO_2 composite films

Figure 5. FTIR spectra of SiO_2 (a), TiO_2 (b) and SiO_2-TiO_2 (c) films. Broad bands between 3600 and 2800 cm^{-1} in all the three spectra can be assigned to fundamental stretching vibration modes of different OH hydroxyl groups (free or bounded).The band at ~960 cm^{-1} is attributed to stretching mode of non-bridging oxygen atoms, e.g., Si-OH and Ti-OH. In (a) and (c), the shoulder at 3650 cm^{-1} is derived from SiO-H stretching. In (b) and (c), the band at 3737 cm^{-1} can be ascribed to surface Ti-OH groups.

Figure 6. (a) Frequency responses of SAW sensor based on SiO_2, TiO_2 and SiO_2-TiO_2 films to 10 ppm NH_3. (b) Electrical response of the SiO_2, TiO_2 and SiO_2-TiO_2 films to 10 ppm NH_3.

Figure 7. Sensing principle of a film with hydroxyl groups. (a) The sensing film in ambient air, H_2O is absorbed on the film. (b) Variation 1: NH_3 is absorbed in the H_2O on the film. (c) Variation 2: the film is catalyzed to condensation by NH_3.

Figure 8. Response of SAW sensors based on based on SiO_2 (a), TiO_2 (b) and SiO_2-TiO_2 (c) films to 10 ppm NH_3 under in the environment with different relative humidity. (d) Comparison of the frequency response and recovery process to10 ppm NH_3 with RH = 40% between the SAW sensors based on SiO_2, TiO_2 films.

Figure 9. (a) Dynamic Frequency responses to NH_3 of various concentrations for the sensor based on SiO_2-TiO_2 films film. (b) Frequency response as a function of NH_3 concentration. (c) Response and recovery times as a function of NH_3 concentration. (d) The dynamic response and recovery of the sensor based on SiO_2-TiO_2 film to various gases. (e) The dynamic response and recovery of the sensor based on SiO_2-TiO_2 film to NH_3 of 10 ppm for 4 cycles. (f) The frequency shift of the sensor based on SiO_2-TiO_2 film to NH_3 of various concentrations in 50 days.

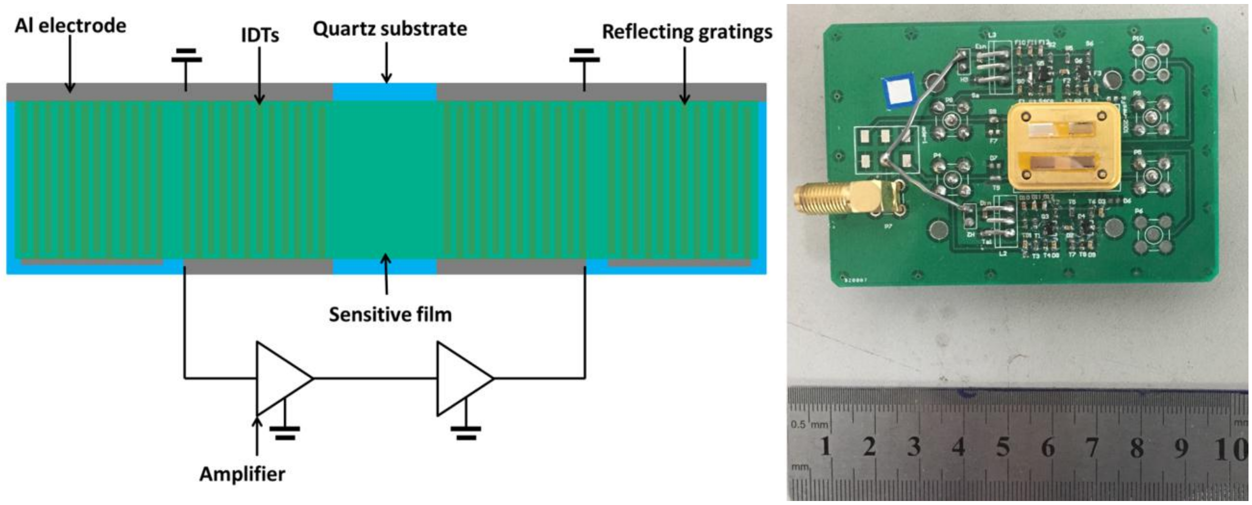
Al electrode
IDTs
Quartz substrate
Reflecting gratings
Sensitive film
Amplifier


SAW sensor
test chamber

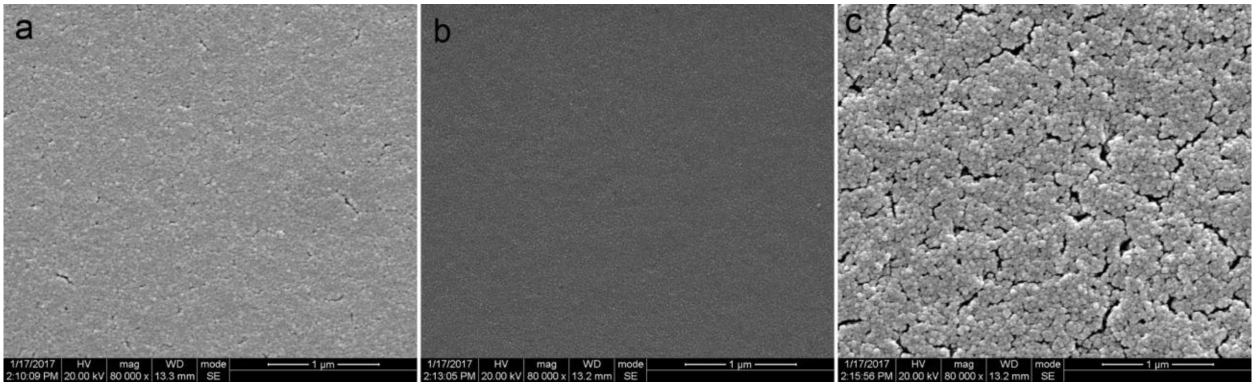
a
b
c

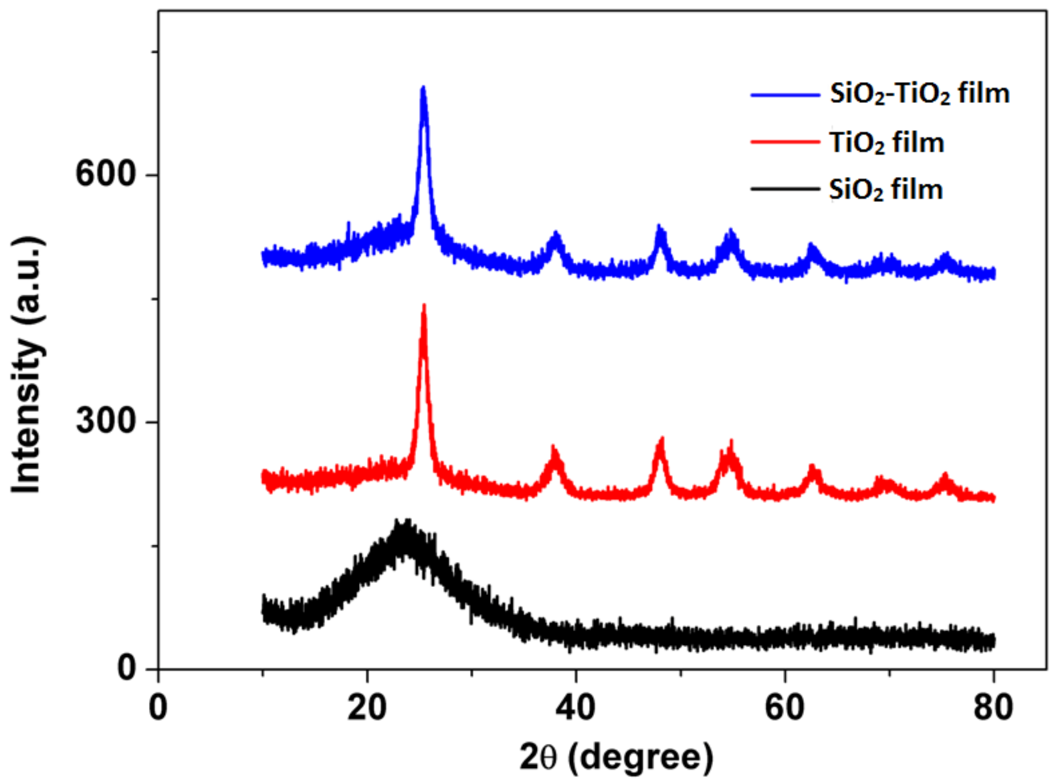

SiO2-TiO2 film
TiO2 film
SiO2 film
Intensity (a.u.)
600
300
0
0
20
40
60
80
2θ (degree)

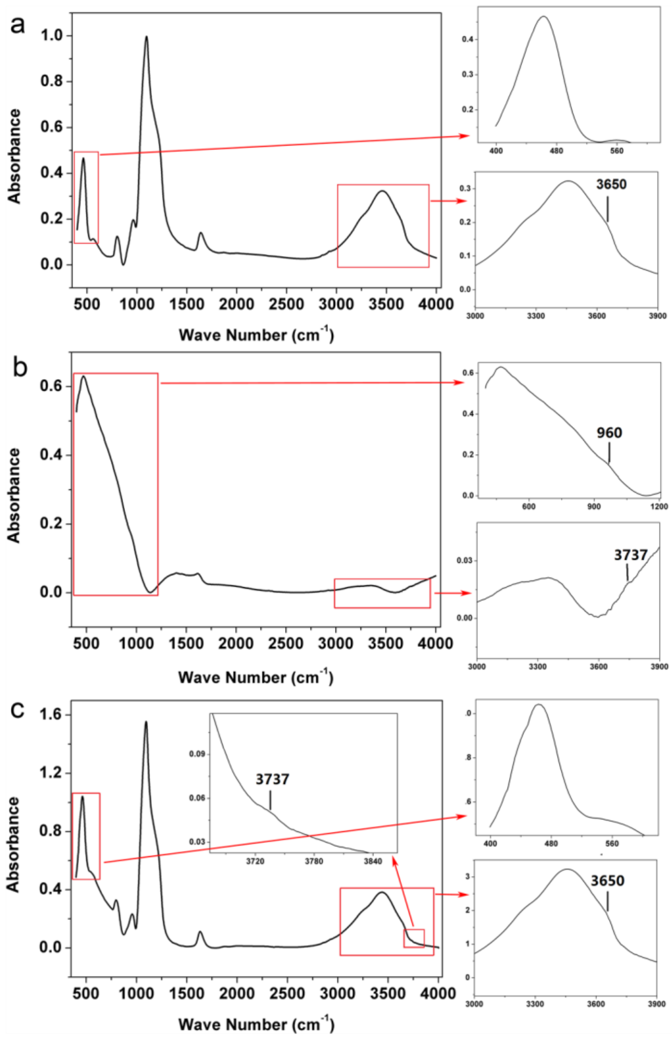
a
b
c
Absorbance
Wave Number (cm-1)
3650
960
3737
3737
3650

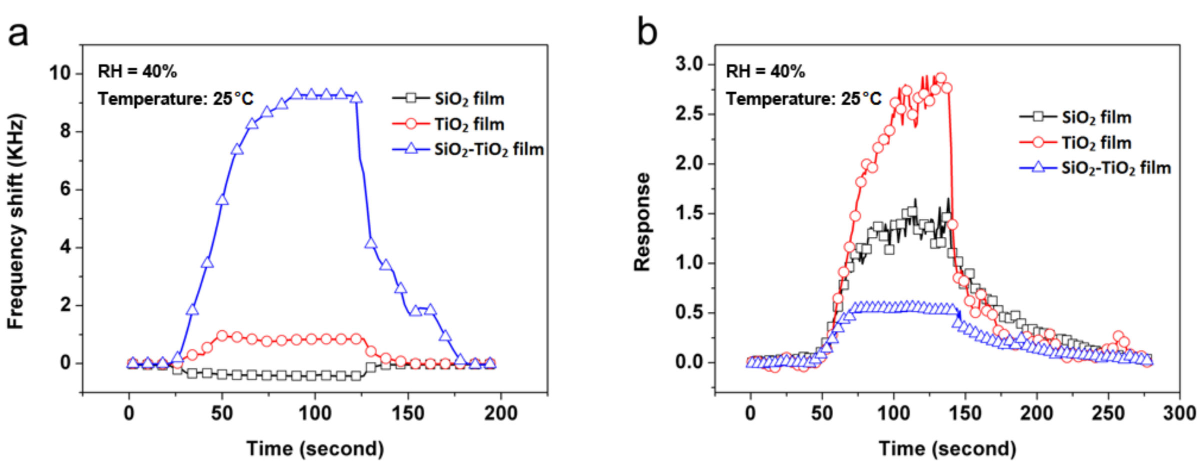
a
RH = 40%
Temperature: 25°C
SiO2 film
TiO2 film
SiO2-TiO2 film
Frequency shift (KHz)
Time (second)
b
RH = 40%
Temperature: 25°C
SiO2 film
TiO2 film
SiO2-TiO2 film
Response
Time (second)

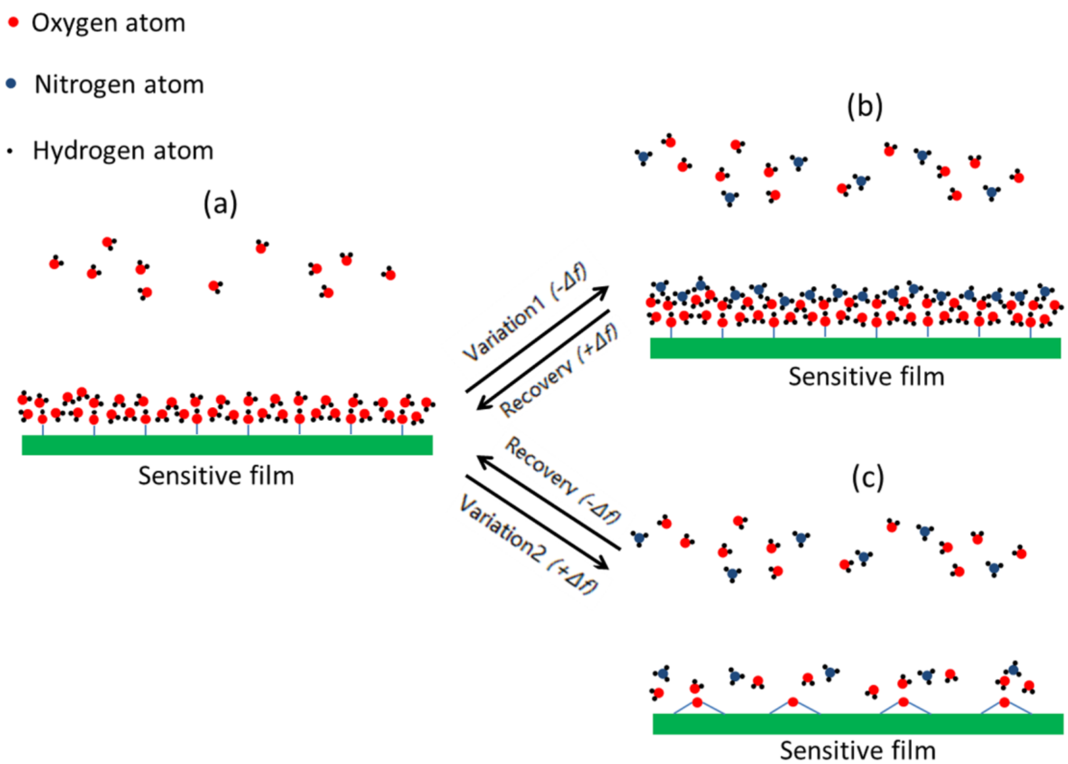

Oxygen atom
Nitrogen atom
Hydrogen atom
(a)
(b)
(c)
Sensitive film
Sensitive film
Sensitive film
Variation1 (-Δf)
Recovery (+Δf)
Recovery (-Δf)
Variation2 (+Δf)

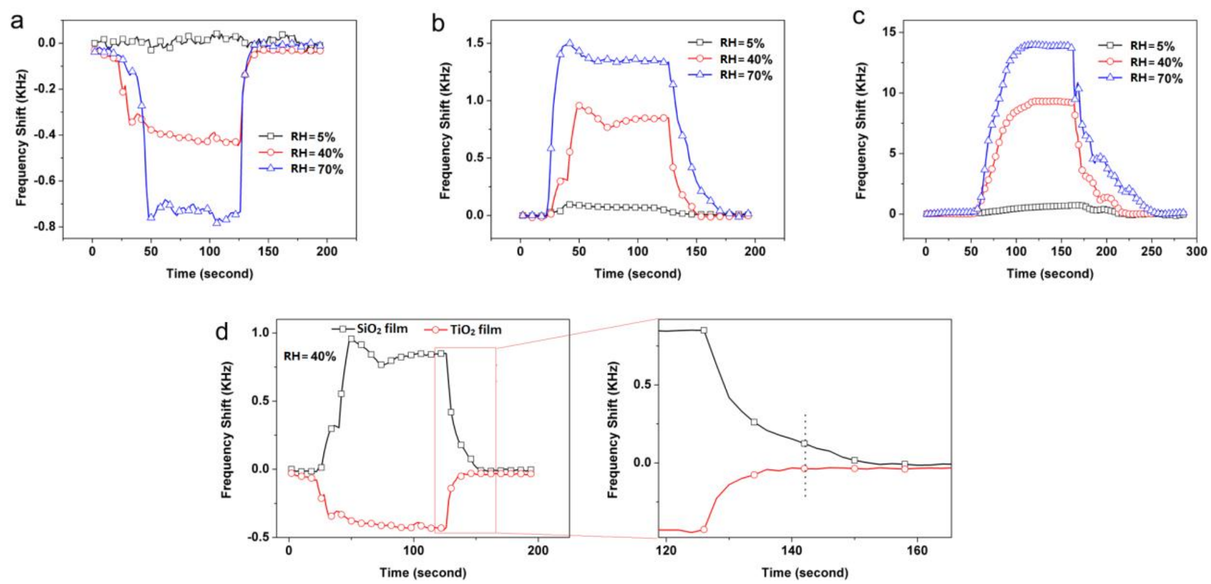

a
b
c
d
Frequency Shift (KHz)
Time (second)
RH = 5%
RH = 40%
RH = 70%
RH = 40%
SiO2 film
TiO2 film

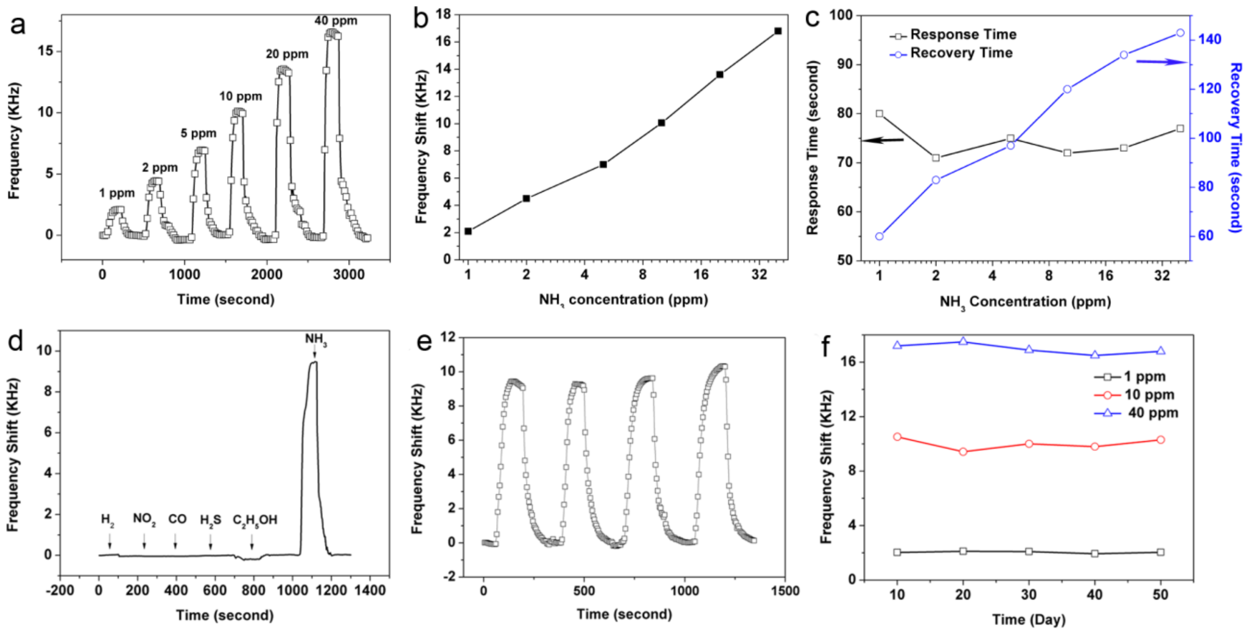

a
Frequency (KHz)
Time (second)
1 ppm
2 ppm
5 ppm
10 ppm
20 ppm
40 ppm
b
Frequency Shift (KHz)
NH3 concentration (ppm)
c
Response Time (second)
Recovery Time (second)
Response Time
Recovery Time
NH3 Concentration (ppm)
d
Frequency Shift (KHz)
Time (second)
H2
NO2
CO
H2S
C2H5OH
NH3
e
Frequency Shift (KHz)
Time (second)
f
Frequency Shift (KHz)
Time (Day)
1 ppm
10 ppm
40 ppm

Table 1. Measured thickness and sheet conductivity of SiO_2, TiO_2 and SiO_2-TiO_2 films.

Film	Thickness (nm)	σ_{sa} (S/square)	σ_{sg} (S/square)	V_0C_s/σ_{sa}	V_0C_s/σ_{sg}	Δf_e (Hz)
SiO_2 film	212	3.2×10^{-12}	8×10^{-12}	49343	19737	4.2×10^{-5}
TiO_2 film	197	0.8×10^{-10}	2.9×10^{-10}	2012	544	6.7×10^{-2}
SiO_2-TiO_2 film	193	0.7×10^{-10}	1.0×10^{-10}	2299	1532	5×10^{-3}

Note: σ_{sa} = Sheet conductivity of the film in ambient air; σ_{sg} = Sheet conductivity of the film in 10 ppm NH_3; Δf_e = frequency shift contributed from electrical loading effect

Table 2. Variation of frequency when RH varies.

Relative Humidity Variation	Frequency Shift (KHz)		
	Sensor1	Sensor2	Sensor3
From 5% to 40%	-10.2	-1.1	-6.3
From 40% to 70%	-7.5	-0.71	-4.8